Integrating Location and Tissue Type Information in Entropy-Based Coupled Object Segmentation of Brain Structures

Alireza Akhondi-Asl[1,2,3], *Hamid Soltanian-Zadeh*[1,2,3]

[1]Control and Intelligent Processing Center of Excellence (CIPCE), School of Electrical and Computer Engineering , University of Tehran, Tehran, Iran
[2]School of Cognitive Sciences, Institute for Studies in Theoretical Physics and Mathematics (IPM), Tehran, Iran
[3]Image Analysis Lab. Radiology Dept., Henry Ford Health System, Detroit, Michigan, USA
a.akhondi@ece.ut.ac.ir, hszadeh@ut.ac.ir

Abstract: *We propose a three-dimensional, nonparametric, entropy-based, coupled, multi-shape approach to segment subcortical brain structures from magnetic resonance images (MRI) using tissue type and location information. It integrates geometrical relationships among different structures into the algorithm by coupling them. It defines an entropy-based energy function which is minimized using quasi-Newton algorithm. To this end, the required probability density functions (pdf) are estimated iteratively using nonparametric Parzen window method. Also, using FANTASM tissue segmentation, a scaled pdf is defined for the tissue type of each structure. In addition, based on the training datasets, a pdf is defined for the location of each structure. Results are given for the segmentation of caudate, thalamus, putamen, pallidum, hippocampus, and amygdale illustrating superior performance of the proposed method compared to those of previous methods*

Keywords: Image segmentation, brain structures, location and tissue type information, medical image processing, magnetic resonance imaging (MRI).

1 Introduction

A major category of the methods proposed for the segmentation of the brain structures from magnetic resonance images (MRI) optimizes an energy function with several parameters that represents the underlying shapes. An exciting approach for the optimization of the energy function is based on the partial differential equations. These equations are defined from the derivatives of the energy function with respect to the model parameters. Kass et al [1] introduced the first work in this category which has been improved by others in recent years. Recent methods benefit from a priori knowledge about the structures of interest. This makes the segmentation process robust to the imperfect image conditions [1]-[4]. For the methods developed based on the a priori information, a registration process is essential to integrate the prior model into the segmentation process.

In addition, the anatomical structures in the brain are related to the neighboring structures through their location, size, orientation, and shape. An integration of these relations into the segmentation process improves accuracy and robustness as shown in [5]-[12]. The 3D deformable model introduced in [5] assumes multivariate Gaussian statistics for the parameters of the coupled shape model of multiple structures. Litvin et al [6] introduced shape distribution as a new concept for the segmentation of coupled objects. Their prior shape model is constructed from a family of shape distributions of features related to the shape. Their method is 2D and its extension to 3D is not reported yet. Addition of new terms in their energy function leads to challenges in the calculation of the derivatives required for the curve evolution. Akselrod-Ballin

et al [7] proposed a knowledge-based multi-scale segmentation method that applied a graph representation in different levels. They used the probabilistic information derived from an atlas and a likelihood function estimated from the training datasets.

Tu et al [8] developed a hybrid method that applied a multiclass classifier for the learning/computing of the multiclass discriminative models and a learned edge field to constrain the region boundaries. Bazin et al [9] introduced a segmentation method that used a statistical and topological atlas generated from the training data and some pre-existing general atlases. This topological atlas used principal component analysis (PCA) to extract shape variability for each structure. Development of the topological atlas requires manual editing and is thus semi-automatic. The authors extended the energy function introduced in the FANTASM method [10] to include this information [9]. Corso et al [11] proposed a graph shifts algorithm using a dynamical hierarchical representation of the image. They minimized an energy function to segment the image. The terms in the energy function were learned from the training data. Tsai et al [12] proposed a segmentation method that used PCA to capture the variability of different structures. Akhondi-Asl et al [13] extended their methods to consider a more realistic shape variability model and an online pdf estimation approach.

In this paper, we add the idea of using tissue type and location information in the method of [13] and extend it by: 1) improving the flexibility of the shape models; 2) applying new fuzzy clustering for the extraction of the tissue type information; 3) construction of a spatial probability density function (pdf) from the training datasets; 4) enhancing the model construction process; and 5) an initialization strategy to improve the quality of the segmentation.

2 Energy Function Construction

There are many features that can be used to identify specific structures in an image. The goal of an automatic segmentation algorithm is to model these features and design the problem in a well-defined mathematical framework. Unfortunately, implementation and/or modeling of these features are not straightforward. Many of the segmentation methods consist of two important parts: a shape descriptor to show the shape; and an energy function to extract the forces to deform the shape. Desirable features are considered in one or both of these parts. Several shape descriptors are used in the literature [14]-[16]. In [14], kernel integrals are used for shape representation. In [15], medial shape representation is used and in [16] a point based method is introduced. More powerful methods for shape representation are based on distance functions and implicit representations. An implicit parametric shape representation has advantages such as computational efficiency, accuracy, capturing wide range of shape variability, and handling topological changes. We use a distance map for shape representation which is zero on the boundary of a shape and the Euclidian distance from the boundary elsewhere (negative inside, positive outside) [1].

2.1 Shape Relations

There are many relationships among different shapes, including pose, orientation, and other geometrical relations [17],[18],[19],[13]. Colliot et al [17] use fuzzy forces to describe spatial relation of different structures Scherrer et al [18] use location constraints provided by fuzzy descriptors as a priori anatomical knowledge to improve the segmentation results. Ciofolo et al [19] use a fuzzy decision system that combines the a priori knowledge extracted from an anatomical atlas with the intensity pdf of the image and positions of the contours relative to one another to have a segmentation method. Akhondi-Asl et al [13] developed a three-dimensional, nonparametric, entropy-based, and multi-shape method that benefits from coupling of the shapes. Their proposed method uses principal component analysis (PCA) to develop shape models that capture structural variability and integrates geometrical relationship among different structures into the algorithm by coupling them (limiting their independent deformations).

We use their methodology for shape relation extraction with a modification on the registration method. We first apply a similarity transformation and then an affine transformation for the fine tuning of the registration process. In [13], only a similarity transformation has been used which cannot align structures accurately.

Suppose that we are interested to segment m structures and have n training datasets where these structures have been segmented by an expert. After extraction of the distance maps of the m desired structures for n different training datasets, we subtract the mean distance map of each structure, computed by averaging of the training datasets, from each of the n signed distance maps

to remove similar parts in different shapes and show them with $\tilde{\psi}_i^k$.

We generate up to *n* different eigenshapes for each of the *m* structures, denoted by ϕ_i^k [13]. Each one of these eigenshapes includes the relationships among different structures and takes the coupling into account. This is because the data from all structures are used in the definition of the eigenshapes. To allow limited, robust shape variability, we use $q \le n$ eigenvectors to represent each shape adaptively. The threshold q is determined based on the sum of the variances in different directions.

In addition, to consider pose differences, we add 12 local alignment parameters (affine transformation) to the shape parameters of each structure. Finally, for each structure, we may write

$$\phi^k\left[\mathbf{w},\mathbf{p}^k\right](x,y,z)=\bar{\Phi}^k\left(\tilde{x}_k,\tilde{y}_k,\tilde{z}_k\right)+\sum_{i=1}^{q} w_i\phi_i^k\left(\tilde{x}_k,\tilde{y}_k,\tilde{z}_k\right) \quad (1)$$

where $\mathbf{w}$ is the vector of eigenvectors multipliers and p^k is the vector containing 12 transformation parameters for the alignment of the *k*th structure.
In the next section, we present our proposed entropy-based segmentation method using the shape model described above.

2.2 Energy Function

There is a variety of information sources that can be used in the segmentation process. The common goal of a segmentation method is to use multiple sources of information without adding unwanted complexity to the method. In addition, because almost all of the segmentation methods are implemented as an optimization process, the initialization is critical for them. In our method, 3 different and independent types of information are used. They are the information about the locations of the structures, the information about the tissue types of the structures (the intensity ranges of the structures), and the intensity uniformity of the structures. The location information is extracted from the training datasets and the tissue type (intensity) information is extracted from the image to be segmented. To this end, two pdf's are estimated for the location and the tissue type of each structure. As explained next, these pdf's are used along with an estimated pdf of the current segmentation of the structure to define an entropy function which is minimized when the image intensities in each structure are uniform.
To segment *m* coupled structures with closed boundaries, there are *m* regions for these structures. We set the area outside of the *m* structures as $m+1$ and use this notation throughout the paper. The energy function is defined as $J\left(\Omega_1,\ldots,\Omega_{m+1}\right)=\left|\Omega\right|\sum_{j=1}^{m+1} P_{\Omega_j}\hat{H}\left(\Omega_j\right)$ where $|\Omega|$ represents the cardinality of the set Ω (number of pixels). When all of the regions are as uniform as possible and are in the correct tissue as much as possible, and also are in the correct location, the energy function is at its minimum. We estimate the entropy of the *k*th structure using $\hat{H}\left(\Omega_k\right)=\frac{-1}{\left|\Omega_k\right|}\int_{\Omega_k}\ln\left(\hat{p}_k\left(\mathbf{x}\right)\times p_{fk}\left(\mathbf{x}\right)\times p_{sk}\left(\mathbf{x}\right)\right)d\mathbf{x}$ where $P_{\Omega_k}=\left|\Omega_k\right|/\left|\Omega\right|$ based on several previous publications [20]. In the entropy estimation, $\hat{p}(\mathbf{x})$ is the approximate pdf in region k of the 3D image I and $p_{fk}(\mathbf{x})$ is the pdf of the tissue type of the region k. Moreover, $p_{sk}(\mathbf{x})$ is the pdf of the location of the *k*-th structure.
We estimate pdf's using the Parzen window method [21], with the Gaussian kernel (K) as $\hat{p}(\mathbf{x})=\hat{p}\left(I(\mathbf{x}),\Omega\right)=\frac{1}{|\Omega|}\int_{\Omega}K\left(I(\mathbf{x})-I(\hat{\mathbf{x}})\right)d\hat{\mathbf{x}}$. We apply the rule of thumb proposed by Silverman [22] to estimate the standard deviation of the Gaussian kernel adaptively.

The second pdf is extracted from a fuzzy clustering method. Fuzzy clustering is a popular method in the literature for classification of the brain MRI into white matter (WM), gray matter (GM), and cerebrospinal fluid (CSF). Our experiments show that a structure may partially belong to different tissue types and also the ranges of the intensities may be completely different in different structures. To consider this information, we use a new strategy where we apply the clustering twice with 3 and 10 clusters using the FANTASM method. We use this method because it considers the information of the neighboring voxels for the clustering. In the next step, equation (2) is used to find the pdf for each of the structures in the 10 class labeled image (I_f) using Fig. 1. In this equation, $C_n(k)$ shows the intensity of the center of the *k*-th label in the *n*-label classification and the parameters l_1 and l_2 are from Table 1 for each structure.

$$\begin{cases} L1=\arg\min\limits_{1\le i\le 10} abs\left(C_3(2)-C_{10}(i)\right)+l_1 \\ L2=\arg\min\limits_{1\le i\le 10} abs\left(C_3(3)-C_{10}(i)\right)+l_2 \end{cases} \quad (2)$$

For the region outside all of the *m* structures (region *m+1*), if all of the other structures have the same pdf, we use *1-p* for the

pdf of the outside region but if there are different pdf's, we use p = 0.5, as described in equation

$$p_{fm+1}(\mathbf{x}) = \begin{cases} 1 - p_{f1}(\mathbf{x}) & \forall k,k',\ p_{fk}(\mathbf{x}) = p_{fk'}(\mathbf{x}) \\ 0.5 & otherwise \end{cases} \quad (3)$$

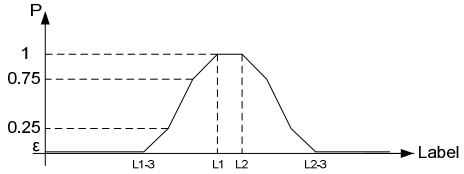

Fig. 1. Probability distribution (scaled) used for the fuzzy membership labels.

Table 1. Shift values used for the probability construction for different structures.

Structure	l_1	l_2
Thalamus	+1	-1
Caudate	+1	-2
Hippocampus	0	-2
Amygdala	-1	-2
Putamen	+1	-1
Pallidum	+3	0

Suppose that there is a dataset (test dataset) and the goal is to segment *m* structures. As explained before, in the first step, it should be registered on the reference dataset. The problem is that the labels are unknown and thus the intensity images should be registered. In this case, a normalized mutual information measure is used as the metric and the linear interpolator is used for interpolation. To improve the results, the skull is stripped from the images using the BET method [23]. If the same process is done for the training datasets, effective information about the locations of the structures in the test datasets can be obtained. To use this information, the same registration protocol is applied on all of the training datasets to find the locations of the structures when the intensity images are used. Next, the strategy explained before for shape model extraction is applied to find the mean shape of each structure ($\bar{\Phi}_I^{\,k}(\mathbf{x})$).

Clearly, $\bar{\Phi}_I^{\,k}(\mathbf{x})$ is negative for the voxels inside the mean structure, is zero on the boundary, and is positive outside. If for a point, this value is more negative than another one, it means that it is more inside the structure and/or is inside the structure in more number of the training datasets than the other one. In addition, the points on the boundary are neither inside nor outside. Thus, the following decreasing function of $\bar{\Phi}_I^{\,k}(\mathbf{x})$ which is 1 for the minimum of $\bar{\Phi}_I^{\,k}(\mathbf{x})$ and is 0.5 for $\bar{\Phi}_I^{\,k}(\mathbf{x}) = 0$ (boundary voxels) is defined.

$$p_{sk}(\mathbf{x}) = \ln\left(\left(e - e^{.5}\right)\left(\bar{\Phi}_I^{\,k}(\mathbf{x}) \Big/ \min\left(\bar{\Phi}_I^{\,k}(\mathbf{x})\right)\right) + e^{.5}\right) \quad (4)$$

Here, for the region outside all of the structures, we find *1-p* for all of the structures and use their minimum for constructing the pdf of this region. The resulting functions can be considered as scaled pdf's.

Finally, we write the energy function as:

$$J(\Omega_1,\ldots,\Omega_{m+1}) = J(P) = \sum_{j=1}^{m+1} -\int_{\Omega_j} \ln\left(\hat{p}_k(\mathbf{x}) \times p_{jfk}(\mathbf{x}) \times p_{sk}(\mathbf{x})\right) d\mathbf{x} \quad (5)$$

where P is the vector of $m \times 12 + q$ parameters (because each one of the local alignments have 12 parameters).

3 Initialization and Optimization

There are many ways to minimize the energy function. Quasi-Newton methods use the observed behavior of the energy function and its gradient to build the curvature information and make an approximation to the Hessian matrix. To minimize the energy function, we use Quasi-Newton algorithm with BFGS method for Hessian matrix estimation [24].

The gradients can be estimated using numerical methods but analytical computation is more robust and generates more accurate results. There are two types of parameters, $\mathbf{w}$ and $\mathbf{p}^k$, for the *i*th component of $\nabla_{\mathbf{w}}$ and $\nabla_{\mathbf{p}^k}$. We compute derivatives as follows.

$$\begin{aligned} \frac{\partial J}{\partial \mathbf{w}_i} = \sum_{j=1}^{m} \int_{\Gamma_j} \frac{\partial \phi_j(\hat{x})}{\partial \mathbf{w}_i} \times \Big\{ & \ln\left(\hat{p}_j(\hat{x}) \times p_{fj}(\hat{x}) \times p_{sj}(\hat{x})\right) \\ & - \ln\left(\hat{p}_{m+1}(\hat{x}) \times p_{fm+1}(\hat{x}) \times p_{sm+1}(\hat{x})\right) \\ & + \frac{1}{|\Omega_j|} \times \int_{\Omega_j} \left(K\left(I(x) - I(\hat{x})\right) \Big/ \hat{p}_j(x)\right) dx \\ & - \frac{1}{|\Omega_{m+1}|} \times \int_{\Omega_{m+1}} \left(K\left(I(x) - I(\hat{x})\right) \Big/ \hat{p}_{m+1}(x)\right) dx \Big\} d\hat{x} \end{aligned} \quad (6)$$

It can be seen that in these two equations, the first two terms show the energy changes due to the changes of the shape for the estimated pdf's for all of the regions. The third and forth terms are the effects of the changes of the shape on the estimated pdf's and the energy function, respectively. We can see that spatial and fuzzy probabilistic distributions do not contribute in these two terms. This is because of the property of the *ln* function that translates multiplication of the probabilities to their summation. In addition, note that all of the desired changes are on the boundaries. In these equations, for all of the points on the boundaries, if the probability of a point to be in the outside region is larger, the energy function is more negative. Also, note that the same happens for the third and

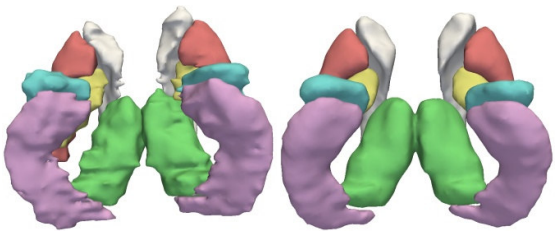

(a) (b)

Fig. 2. Segmentation comparison between manually segmented structures (a) and the structures segmented by the proposed algorithm (b).

forth terms. Using the current parameters, the pdf's, $\frac{\partial \phi^k(\mathbf{x})}{\partial p_i^k}$ and $\frac{\partial \phi^k(\mathbf{x})}{\partial w_i}$ can be estimated iteratively using the method of [13]

As stated previously, the initialization is an important part of the segmentation process. So far, the model and the optimization function of the model are established. The next step is to place the model in the correct location of the image and start the optimization. For this purpose, we use the center of mass of $Ib_k = \begin{cases} 1 & \bar{\Phi}_I^k(\mathbf{x}) \le 0 \\ 0 & \bar{\Phi}_I^k(\mathbf{x}) > 0 \end{cases}$ for pose initialization. Then, we use the spatial and fuzzy information to find the best location of each structure individually using the following energy function where d is the translation vector.

$$E_j = -\int_{\Omega_j} p_{f\,j}(\hat{x}+d) \times p_{s\,j}(\hat{x}+d)\, d\hat{x}$$

$$\frac{\partial E_j}{\partial d_i} = \iint_{\Gamma_j} \frac{\partial \phi_j(\hat{x}+d)}{\partial d_i} \times p_{f\,j}(\hat{x}+d) \times p_{s\,j}(\hat{x}+d)\, d\hat{x} \quad (7)$$

These translations are used in the final optimization step described before. We do not use intensity information in this step because the initial position is such that the estimated pdf is inaccurate. We use the intensities inside each region in final state of this step for the estimation of the variance and we fix it during the segmentation process.

4 Results

In this section, we present the results of applying the proposed method to real MRI of the human brain. The MRI data are obtained from 2 different sources. As the main dataset, the Internet Brain Segmentation Repository (IBSR) [25] is used for training and testing of the proposed method. There are 18 datasets on which expert physicians have segmented 43 brain structures. Same preprocessing that has been used in [13] is used here. To evaluate the results, we use the Dice coefficient (k), the Hausdorff distance (H), and the mean distance (M) [9]. Due to the outliers, the 95 percentile of the Hausdorff distance is used (H_{95}). For 3D visualization of the structures, we use 3D Slicer and for registration of the training and testing datasets, we use ITK library. For optimization and extraction of the principal shapes, we use MATLAB.

For the IBSR dataset, among different structures in the brain, we work with the following 6 structures on the two hemispheres for a total of 12 structures: 1) caudate; 2) thalamus; 3) putamen; 4) pallidum; 5) hippocampus, and 6) amygdale. These structures are either used in many applications or hard to segment because of their unclear boundaries. They include a variety of shapes with different signal intensities, sizes, and other geometrical features. We use the leave-one-out strategy to test the proposed segmentation algorithm. We randomly use one of the datasets as the reference to remove any bias due to this process.For this specific dataset, we used another random dataset as the reference. We segment the left and right structures or multiple structures by the proposed coupling method.

Table 2. performance measures for the segmentation of the structures.

	Thalamus	Putamen	Caudate	Pallidum	Hippocampus	Amygdala
Our Method						
k	0.85±0.04	0.80±0.06	0.78±0.04	0.75±0.05	0.71±0.06	0.68±0.09
M	0.75±0.22	0.72±0.23	0.61±0.14	0.74±0.19	0.84±0.18	0.78±0.29
H_{95}	2.38±0.65	2.32±0.63	2.17±0.51	2.38±0.69	2.62±0.63	2.99±0.94
[13]k	0.83±0.04	0.81±0.05	0.75±0.06	0.74±0.05	0.69±0.06	0.52±0.13
Bayes [7]						
k	0.84	0.79	0.80	0.74	0.69	0.63
M	1.44	1.6	1.44	1.43	1.88	1.67
H_{95}	2.9	3.36	3.07	2.75	4.57	3.38
Naive [7]						
k	0.83	0.77	0.65	0.72	0.62	0.65
ISCA [7]						
k	0.80	0.78	0.74	0.70	0.64	0.58
M	1.55	1.72	1.84	1.55	1.91	1.78
H_{95}	3.2	3.89	4.46	3.2	4.44	3.89
[19]						
k	0.77	0.70	0.65	0.62	-	-
M	1.70	1.46	1.71	1.51		
[9]*k*	0.78±0.05	0.76±0.03	0.80±0.04	-	-	-

In Fig. 2, a sample segmentation of the selected structures by our coupled method is shown along with the expert segmented structures.

Evaluation of the results using the *k, M*, and H_{95} for the selected structures for 18 datasets is shown in Table 2. This table lists the performance measures for the segmentation of these structures by the proposed method which considers the coupling information. Besides, it lists the segmentation results of 6 other popular methods that have reported results for the IBSR datasets. It

shows that our method is more accurate than the others for Thalamus, putamen, pallidum, hippocampus, and amygdale. Results of the caudate segmentation shows that our method is superior to the others based on M and H_{95} but is inferior to the methods of Bazin et al [9] and Akselrod et al [7] for the k. Comparing our method with the method of Akselrod et al [7] (as the nearest method to ours) shows that our method produces superior results for M and H_{95}. For example, for caudate our method has M value of 0.61 mm which is about 2.5 times better than that of the Akselrod et al [7] method. In addition, our method is superior to their method based on k for all of the structures expect caudate.

5 Conclusion

We have presented a new method for the segmentation of the brain subcortical structures using their shape relationships. In the model development phase, the proposed method registers each structure individually before estimating their shape variations in two steps using similarity and affine transformations. In addition, in the segmentation phase, the proposed method applies an independent transformation to each structure, improving flexibility of the segmentation model. The transformation has twelve parameters to implement appropriate rotation, scaling, translation, and shearing. The energy function used for the segmentation is based on the entropy of different structures. With an automatic initialization of the structures and use of the quasi-Newton algorithm, a local minimum of the energy function is found. Fuzzy tissue type and location information are used to generate robust and accurate segmentations. Experimental results have illustrated quality of the results generated by the proposed framework with respect to the competitive methods in the literature.

References

1. Kass M., Witkin A., Terzopoulos D.: Snakes: Active Contour Models. In:First International Conference on Computer Vision, pp. 259-268, (1987)
2. Leventon M. E., Grimson W. E. L., and Faugeras O.: Statistical Shape Influence in Geodesic Active Contours. In: IEEE Internatinal Conference on Computer Vision and Pattern Recognition, 1, 1316--1323 (2000)
3. Jehan-Besson S., Herbulot A., Barlaud M., and Aubert G.: Shape Gradient for Image and Video Segmentation, Mathematical Models in Computer Vision: The Handbook, Springer, (2005)
4. Pohl K. M., Fisher J., Kikinis R., Grimson W. E. L., and Wells W. M.: Shape Based Segmentation of Anatomical Structures in Magnetic Resonance Images, In: International Conference on Computer Vision, 3765, 489—498 (2005)
5. Yang J., Staib L. H., and Duncan J. S.: Neighbor-Constrained Segmentation with Level Set Based 3D Deformable Models, IEEE Transactions on Medical Imaging, 23, 940--948, (2004)
6. Litvin A. , and Karl W.C.: Coupled Shape Distribution-Based Segmentation of Multiple Objects. Tech. Rep. ECE-2005-01, Boston University, Boston, USA (2005)
7. Akselrod-Ballin A., Galun M., Gomori J. M., Brandt A., and Basri R.: Prior knowledge driven multiscale segmentation of brain MRI. In: MICCAI, 10, 118--126 (2007)
8. Tu Z., Toga A. W.: Towards whole brain segmentation by a hybrid model. In:MICCAI, 10, 169--177 (2007)
9. Bazin P. L., Pham D. L.: Homeomorphic brain image segmentation with topological and statistical atlases. Medical Image Analysis, 12, 616--625 (2008)
10. Pham D.: Robust fuzzy segmentation of magnetic resonance images. In: Fourteenth IEEE Symposium on Computer-Based Medical Systems (CBMS), 127--131 (2001)
11. Corso J. J., Tu Z., Yuille A., Toga A.: Segmentation of sub-cortical structures by the graph-shifts algorithm. In: International Conference on Information Processing in Medical Imaging, 20, 183--197 (2007)
12. Tsai A., Wells W., Tempany C., Grimson E., and Willsky A.: Mutual Information in Coupled Multi-Shape Model for Medical Image Segmentation. Medical Image Analysis, 8, 429—445 (2004)
13. Akhondi-Asl A., Soltanian-Zadeh H.: Effect of Number of Coupled Structures on the Segmentation of Brain Structures. journal of signal processing systems 54 215-230 (2009).
14. Hong B. W., prados E., Soatto S., and vese L.: Shape Representation based on Integral Kernels: Application to Image Matching and Segmentation. In: Proceedings of the 2006 IEEE Computer Society Conference on Computer Vision and Pattern Recognition, 1, 833—840 (2006)
15. Pizer S., Fritsch D., Yushkevich P., Johnson V., and Chaney E.: Segmentation, registration, and measurement of shape variation via image object shape. IEEE Trans. Med. Imaging, 18 851—865 (1999).
16. Cootes T. F., Taylor C. J., Cooper D. H., and Graham J.: Active shape models-their training and application. Comput. Vis. Image Understanding, 61, 38—59 (1995)
17. Colliot O., Camara O., and Bloch I.: Integration of fuzzy spatial relations in deformable models - Application to brain MRI segmentation. Pattern Recognition, 39, 1401-1414 (2006)
18. Scherrer B., Dojat M., Forbes F., and Garbay C.: LOCUS: local cooperative unified segmentation of MRI brain scans. In: MICCAI, 10, 219-227 (2007)
19. Ciofolo C., Barillot C.: Brain segmentation with competitive level sets and fuzzy control. International Conference on Information Processing in Medical Imaging, 19, 333-344 (2005)
20. J. Kim, J. Fisher, A. Yezzi, M. Cetin, and A. Willsky, "Nonparametric methods for image segmentation using information theory," IEEE International Conference on Image Processing, vol. 3, pp. 797–800, 2002.
21. Parzen E.: On the estimation of a probability density function and the mode. Annals of Mathematical Statistics, 33, 1065--1076 (1962)
22. Silverman B. W.: Density Estimation. Chapman & Hall/CRC, London (1986)
23. Smith S.: Fast robust automated brain extraction. Human Brain Mapping, 17, 856--876 (2001)
24. Bathe K. J. and Cimento A. P.: Some Practical Procedures for the Solution of Nonlinear Finite Element Equations. Computer Methods in Applied Mechanics and Engineering, 22, 59-85 (1980)
25. http://www.cma.mgh.harvard.edu/ibsr